Prediction of radiation ratio and sound transmission of complex extruded panel using wavenumber domain finite element and boundary element methods

H Kim[1], J Ryue[1], D J Thompson[2] and A D Müller[2]

[1] School of Naval Architect and Ocean Engineering, University of Ulsan, 93 Daehak-ro Nam-gu, Ulsan, Korea
[2] Institute of Sound and Vibration Research, University of Southampton, Southampton, UK

Email : jsryue@ulsan.ac.kr

Abstract. Recently, complex shaped aluminium panels have been adopted in many structures to make them lighter and stronger. The vibro-acoustic behaviour of these complex panels has been of interest for many years but conventional finite element and boundary element methods are not efficient to predict their performance at higher frequencies. Where the cross-sectional properties of the panels are constant in one direction, wavenumber domain numerical analysis can be applied and this becomes more suitable for panels with complex cross-sectional geometries. In this paper, a coupled wavenumber domain finite element and boundary element method is applied to predict the sound radiation from and sound transmission through a double-layered aluminium extruded panel, having a typical shape used in railway carriages. The predicted results are compared with measured ones carried out on a finite length panel and good agreement is found.

1. Introduction

Nowadays, complex shaped stiffened panels are widely used for many structures such as railway vehicles, ships, offshore structures, etc. in order to make them lighter and stronger. To predict the acoustic performances of these structures, it is essential to understand the vibro-acoustic behaviour of complex shaped panels. As examples of such panels, extruded aluminium panels which have uniform cross-sections along their lengths are considered in this study.

For structures with uniform cross-sections like extruded panels, wavenumber domain analysis becomes more suitable for predicting their vibro-acoustic performance. The radiation ratio and sound transmission loss are important vibro-acoustic features of extruded panels that are investigated in this study. The radiation ratio and sound transmission of extruded panels have been studied by a few researchers using wavenumber domain techniques so far. The radiation ratio for a simple plate strip has been studied theoretically by Xie *et al.* [1] and they proposed simplified formulae for the radiation ratio of plate strips. A numerical analysis for the radiation ratio from and sound transmission through plate strips has been carried out by Prasetiyo [2] using a wavenumber domain numerical method. He found that the numerical results coincided well with the theoretical results for plate strips. For plate strips with longitudinal stiffeners, Orrenius and Finnveden [3] have examined the contribution of the stiffeners in terms of the dispersion relations by using the wavenumber domain finite element method. From their study, it was found that the stiffeners behave like rigid or simply supported boundaries at

high frequencies and then the waves travel only along the strips (or bays) which are bounded by two adjacent stiffeners. Because of that, the dispersion curves of the stiffened plate strip converge to those of bays separated by the stiffeners. Kim and Ryue [4] have predicted the radiation ratio for single and double layered stiffened strip plates numerically and investigated the variation of that caused by the stiffeners and added layer. However, they chose a double layered extruded panel possessing a relatively simple cross-sectional geometry.

In terms of experimental study, Müller [5] has measured the radiation ratio and sound transmission of an extruded panel with a complex geometry, which is a typical floor panel of a railway carriage. Nilsson *et al.* [6] have also measured the sound transmission loss through the extruded panel. In these experiments, Müller mounted the extruded panel in an aperture between two reverberation chambers, while Nilsson *et al.* used the reverberation and anechoic chambers. However, the experimental results have not previously been compared with numerical ones.

In this paper, the radiation ratio and sound transmission loss of an extruded panel used in railway vehicles are investigated using a numerical method, called the wavenumber domain finite and boundary element method (WFE/BE) method. The WFE method has often been used for the vibration analysis of waveguide structures like rails [7, 8] and plates [3], etc. The WFE/BE approach has also been used to predict the sound radiated from rails [9], simple plate strips [2] and stiffened double plates [4]. The numerical results predicted from the WFE/BE method are validated with experiments. In WFE/BE analysis, the panel is assumed to have an infinite length but the experiments are carried out with a finite length extruded panel. Despite this, from the comparison between the simulated and measured results, it is found that the predicted results from the WFE/BE method coincide well with the measured ones, especially at high frequencies.

2. Wavenumber domain finite and boundary elements analysis for an extruded panel

In this section, the wavenumber domain finite element and boundary element (WFE/BE) method is described briefly. This method is known to be particularly useful for waveguide structures which have uniform cross-section along one direction (x direction in this paper), such as rails, plates, ducts, etc. Details of the derivation of the governing equations are well reported in the literature [10] so only a brief introduction of the method is given here. For the WFE/BE analysis in this paper, a software program, called WANDS, developed at ISVR is used to analysis the vibro-acoustic behaviours in the extruded panel numerically.

In this wavenumber domain method, only a 2D cross-section of a structure is meshed, assuming that the cross-sectional deformation travels harmonically along the third direction with respect to time and space. The governing equation of the WFEs for a waveguide structure modelled with plate elements is given by

$$\left\{\mathbf{K}_{s4}(-i\kappa)^4 + \mathbf{K}_{s2}(-i\kappa)^2 + \mathbf{K}_{s1}(-i\kappa) + \mathbf{K}_{s0} - \omega^2\mathbf{M}_s\right\}\tilde{\mathbf{\Phi}} = \tilde{\mathbf{F}}_s \tag{1}$$

where $\mathbf{K}_{s4}$, $\mathbf{K}_{s2}$, $\mathbf{K}_{s1}$, and $\mathbf{K}_{s0}$ are the matrices that come from the stiffness of the structure, $\mathbf{M}_s$ is the mass matrix, ω is the angular frequency, κ is the structural wavenumber along the x direction, $\tilde{\mathbf{\Phi}}$ contains the displacements of the cross-section at the nodes of the FEs and $\tilde{\mathbf{F}}_s$ is the vector of excitation forces at these nodes.

For free vibration, i.e. $\tilde{\mathbf{F}}_s = \mathbf{0}$, equation (1) can be solved for ω at given real wavenumbers (or for κ at given ω). This general eigenvalue problem provides dispersion relations of waves propagating along the x direction of the structure.

When a waveguide structure is connected with fluid, wavenumber domain boundary elements (WBE) are introduced to model the fluid and coupled with the WFEs. If this fluid-coupled structure is excited by mechanical forces $\tilde{\mathbf{F}}_s$ and also acoustic pressures $\tilde{\mathbf{P}}_i$, the governing equations of the WFE/BEs are given by

$$\left\{\mathbf{K}_s(\kappa)-\omega^2\mathbf{M}_s\right\}\tilde{\mathbf{\Phi}}=\tilde{\mathbf{F}}_s+j\omega\rho_0\mathbf{C}_1\tilde{\mathbf{\Psi}} \tag{2}$$

$$\mathbf{H}\tilde{\mathbf{\Psi}}-\mathbf{G}\frac{\partial\tilde{\mathbf{\Psi}}}{\partial\mathbf{n}}=\frac{\tilde{\mathbf{P}}_i}{j\omega} \tag{3}$$

$$\mathbf{I}\frac{\partial\tilde{\mathbf{\Psi}}}{\partial\mathbf{n}}-j\omega\mathbf{C}_2\tilde{\mathbf{\Phi}}=\mathbf{0} \tag{4}$$

where $\mathbf{K}_s(\kappa)=\mathbf{K}_{s4}(-i\kappa)^4+\mathbf{K}_{s2}(-i\kappa)^2+\mathbf{K}_{s1}(-i\kappa)+\mathbf{K}_{s0}$, $\mathbf{C}_1$ denotes the coupling matrix between the WFEs and WBEs, ρ_0 is the fluid density, $\mathbf{H}$ and $\mathbf{G}$ are matrices of Green's functions, while $\tilde{\mathbf{\Psi}}$ and $\frac{\partial\tilde{\mathbf{\Psi}}}{\partial\mathbf{n}}$ are the velocity potential and the normal velocity at the nodes of the boundary elements. $\mathbf{n}$ denotes the normal directional vector of the WBEs, $\mathbf{I}$ is an identity matrix and $\mathbf{C}_2$ is a matrix allocating fluid-coupled dofs in $\tilde{\mathbf{\Phi}}$.

Once $\tilde{\mathbf{\Psi}}$ and $\frac{\partial\tilde{\mathbf{\Psi}}}{\partial\mathbf{n}}$ have been found from equations (2)~(4), the sound pressure $\tilde{p}(\kappa)$ and fluid particle velocity $\tilde{v}(\kappa)$ at the fluid nodes in the wavenumber domain are obtained by

$$\tilde{p}(\kappa)=j\omega\rho_0\tilde{\mathbf{\Psi}} \tag{5}$$

$$\tilde{v}(\kappa)=-\frac{\partial\tilde{\mathbf{\Psi}}}{\partial\mathbf{n}}. \tag{6}$$

These pressures and fluid particle velocities are used in the calculation of sound radiation and transmission later.

3. Application for an extruded panel

3.1. Cross-sectional modelling

In this study, an extruded panel shown in figure 1(a), which is a typical floor panel of a railway

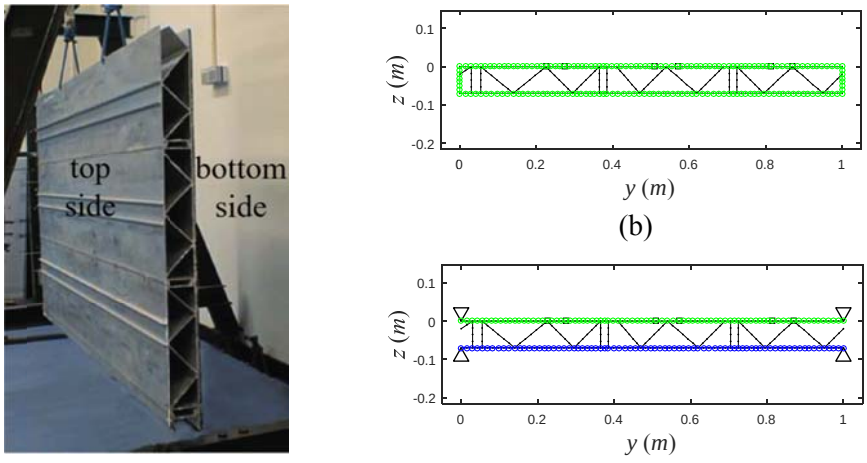

(a) (b) (c)

Figure 1. (a) A specimen of an extruded panel for a railway vehicle. Cross-sectional models of the extruded panel for predicting (b) radiation ratio and (c) transmission loss (Circles indicate WBE nodes and dots are WFE nodes).

Table 1. Properties and dimensions of the extruded panel.

Material	Density (kgm^{-3})	Thickness (mm)	Poisson's ratio	Young's modulus (GPa)
Aluminium	2700	2.54	0.3	70
Rubber	1500	4	-	-

vehicle, is examined by WFE/BE analysis. The panel is made of aluminium but the bottom plate is covered with a rubber mat. The cross-sectional models of the panel structure are illustrated in figure 1(b) and 1(c), composed of plate and beam finite elements. The low height stiffeners attached on the top plate are modelled using beam elements and marked with '□' in figure 1(b) and 1(c). To reflect the attached rubber mat on the bottom plate, the mass and damping of the bottom plate have been increased. The damping loss factor assumed for bare aluminium is 0.005 and for the compound plate is 0.02. The dimensions and properties of the panel are listed in table 1. The air cavity inside the extruded panel is not considered in this study because lots of nodes for modelling the air leads to long calculation time.

In the WFE/BE modelling for the radiation ratio, the panel is set to have free-free boundary conditions at both ends and the boundary elements are placed to enclose the panel entirely as shown in figure 1(b) (BE nodes are marked with '○' in figure 1(b) and 1(c)). In this modelling, it is assumed that the sound radiation from the left and right sides of the panel are negligible so that the WBEs on both sides are set to be rigid in order to simplify the model.

On the other hand, in case of sound transmission, the WBEs are located only on the top and bottom plates as shown in figure 1(c) assuming that each panel is rigidly baffled for $y \le 0$ and $y \ge 1\,\mathrm{m}$. The sound transmission is evaluated from the comparison between the power incident on the panel and that transmitted through the panel. In the experiments, the sound transmission is measured by installing the panel in a wall with a frame between two rooms. Therefore, the practical boundary condition of the panel must be between fixed and simply supported conditions. In the numerical study the simply supported boundary condition is applied at both ends of the panel as illustrated in figure 1(c). The variation induced by different boundary conditions has also been checked and it is found that it only affects at low frequencies.

3.2. Dispersion relation

In order to understand characteristics of waves propagating along the extruded panels shown in figure 1(b) and 1(c), their dispersion diagrams are illustrated in figure 2. The dispersion diagrams shown in

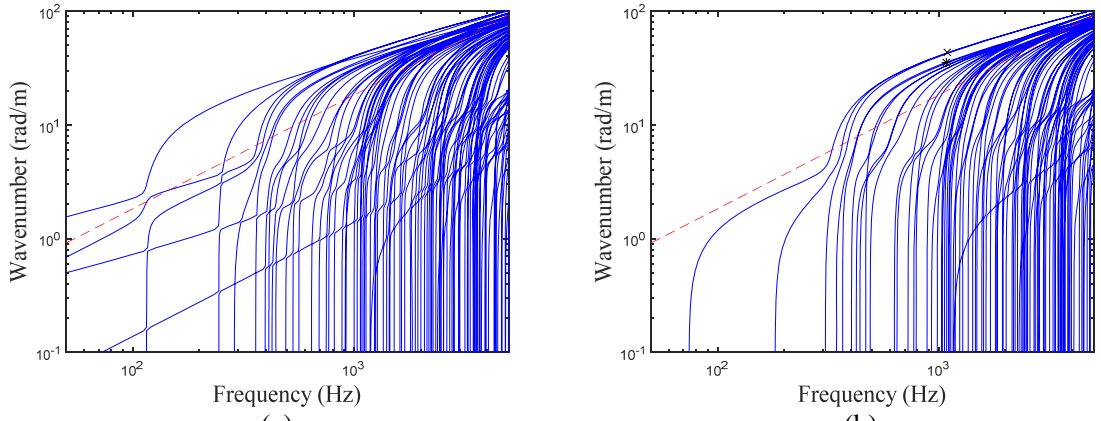

Figure 2. The dispersion diagrams of the extruded panel with (a) free boundary conditions (figure 1(b)) and (b) simply supported boundary conditions (figure 1(c)). (Acoustic wave is added with a dashed line).

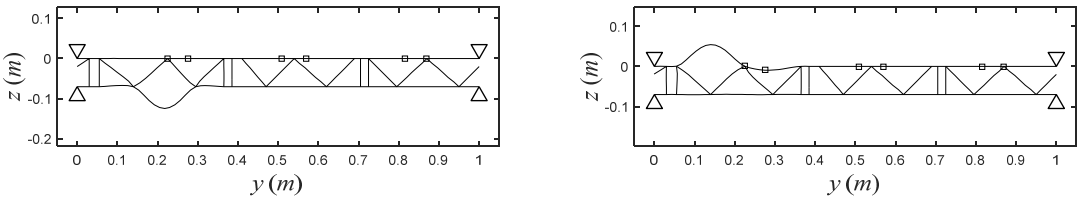

Figure 3. The deformation shapes of two waves marked with (a) '×' and (b) '∗' in figure 2(b).

figure 2(a) and 2(b) are obtained from the panels with the boundary conditions shown in figure 1(b) and 1(c), respectively. For comparison, the acoustic wavenumber is also shown with a dashed line.

As mentioned in Section 3.1, the extruded panel is modelled with different boundary conditions at both ends of the panel for the prediction of radiation ratio and sound transmission. The effects of boundary condition are more obvious in the low frequency range as seen in figure 2. There are several waves at low frequency in the case of the free-free boundary condition, as shown in figure 2(a). These correspond to global modes of the extruded panel. On the contrary, the panel with the simply supported boundary condition does not have any wave below about 75 Hz, as illustrated in figure 2(b), due to the restriction at the boundary; many waves appear from about 300 Hz.

In contrast, at high frequency and high wavenumber, local modes occur in the plate strips and both dispersion diagrams show similar features. It is found that there are two groups of dispersion curves at high wavenumber in figure 2(b). To observe the deformation shapes of these wave groups, cross sections of one wave from each group, marked with '×' and '∗' in figure 2(b), are shown in figure 3. It can be seen that these two waves have a localized deformation restricted within one bay in the top and bottom plates between two adjacent core stiffeners. Since the bottom plate has a larger density than the top plate due to the rubber mat, the wave marked with '×' travels relatively slower than that marked with '∗'.

3.3. Calculation of radiation ratio and sound transmission loss

The radiation ratio (σ) of the structure can be determined as

$$\sigma = \frac{W_{rad}}{\rho_0 c \Gamma \left\langle \overline{v^2} \right\rangle_{\inf}} \tag{7}$$

where c is the sound speed in the fluid, Γ is the perimeter of the cross-section in contact with the fluid and $\left\langle \overline{v^2} \right\rangle_{\inf}$ represents the integral of the mean-square velocity over the length and the average over the width. The radiated power, W_{rad} , and average mean-squared velocity, $\left\langle \overline{v^2} \right\rangle_{\inf}$ of the panel in equation (7) can be obtained as

$$W_{rad} = \frac{1}{4\pi} \mathrm{Re}\left(\int_{-k}^{k} \int_{\Gamma} \tilde{p}^*(\kappa) \tilde{v}(\kappa) d\Gamma d\kappa \right) \tag{8}$$

$$\left\langle \overline{v^2} \right\rangle_{\inf} = \frac{1}{2\pi\Gamma} \int_{-\infty}^{\infty} \int_{\Gamma} \frac{\left| \tilde{v}(\kappa) \right|^2}{2} d\Gamma d\kappa \tag{9}$$

where k is the acoustic wavenumber, $*$ denotes the complex conjugate. Since $\tilde{p}(\kappa)$ and $\tilde{v}(\kappa)$ can be found from equations (5) and (6), equations (8) and (9) can be evaluated with the WFE/BE solutions.

For the calculation of sound transmission in the WFE/BE method, incident waves which excite the

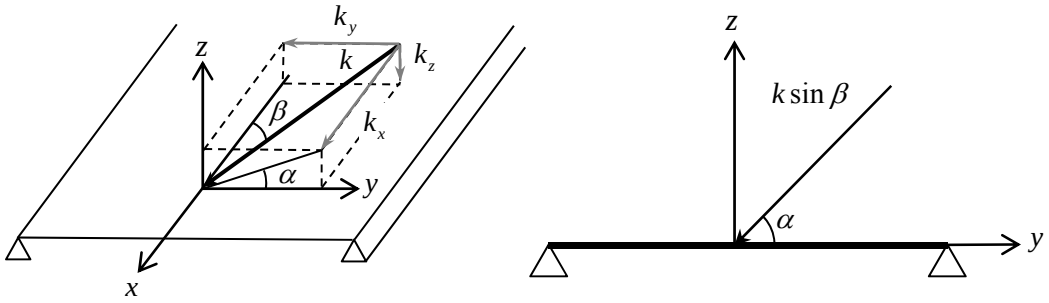

(a) (b)

Figure 4. Coordinates to define a wave incident on the plate (a) in 3D space and (b) in the $y-z$ plane.

extruded panel should be defined. It is assumed that the sound is incident on the top plate with an angle, α, in the $y-z$ plane and an angle, β, about the x-axis, as depicted in figure 4. The acoustic wavenumber of the incident wave can be written as

$$k = \left(k_x^2 + k_y^2 + k_z^2\right)^{1/2} \tag{10}$$

with the directional wavenumbers k_x, k_y and k_z along the x, y and z directions, respectively. These directional wavenumbers can be expressed in terms of α and β as

$$k_x = k\cos\beta \tag{11}$$

$$k_y = k\sin\beta\cos\alpha \tag{12}$$

$$k_z = \left(k^2 - k_x^2 - k_y^2\right)^{1/2}. \tag{13}$$

The incident power, W_i, can be obtained in the wavenumber domain as

$$W_i(\alpha,\beta) = \frac{1}{2}\int_\Gamma \frac{\left|\tilde{p}_i(\kappa)\right|^2 \sin\alpha\sin\beta}{\rho_0 c} d\Gamma \tag{14}$$

For the extruded panel, the transmitted power, W_t, can be calculated as

$$W_t(\alpha,\beta) = \frac{1}{2}\mathrm{Re}\left(\int_\Gamma \tilde{p}_t{}^*(\alpha,\beta)\tilde{v}_t(\alpha,\beta)d\Gamma\right) \tag{15}$$

where $\tilde{p}_t$ and $\tilde{v}_t$ are the sound pressure and fluid particle velocity on the bottom plate. The transmission coefficient, τ, is defined by the ratio between the incident and transmitted powers as

$$\tau(\alpha,\beta) = \frac{W_t(\alpha,\beta)}{W_i(\alpha,\beta)} \tag{16}$$

Since equation (16) applies at specific angles α and β, the transmission coefficient for a diffuse sound field, τ_d, needs to be calculated by [11]

$$\tau_d = \frac{\int_0^{\pi/2}\int_0^{\pi/2} \tau(\alpha,\beta)\sin^2\beta\sin\alpha\, d\alpha\, d\beta}{\int_0^{\pi/2}\int_0^{\pi/2} \sin^2\beta\sin\alpha\, d\alpha\, d\beta} \tag{17}$$

Finally, the sound transmission loss in a diffuse sound field through the panel is determined using

$$R = 10\log_{10}\left(\frac{1}{\tau_d}\right). \tag{18}$$

3.4. Predicted results of radiation ratio and sound transmission loss

In the prediction of radiation ratio, a point force was applied at two different types of locations on the top plate, one in the middle of a strip between two core stiffeners and one where a core stiffener is connected. These positions correspond to P1 (or P2) on the strip and P3 and P4 on the stiffener as specified in Section 4.

The average mean-squared velocity of the top plate and the sound power radiated from the bottom plate are illustrated in figure 5 as image plots against the frequency and wavenumber when a point force is applied at $y = 0.385\,\text{m}$, which is point P3. The acoustic wave is plotted with a dashed line in figure 5(b). It is seen from figure 5(a) that strong vibration occurs due to a couple of global mode waves at frequencies below about 300 Hz, while many waves possessing higher order cross-sectional deformations contribute above about 400 Hz. Although the top and bottom plates can vibrate, they do not radiate sound if κ is bigger than the acoustic wavenumber k. As seen in figure 5(b), global mode waves in the low frequency range do not contribute much to the sound power radiated from the extruded panel.

In the reference [5], it is stated that a vibration mode localized within a bay in the top plate exists above 400 Hz. In order to confirm this feature from the numerical results, the deformation shapes of the top plate at 428 and 653 Hz in the spatial domain are illustrated in figure 6 (these two frequencies are indicated with dashed lines in figure 5(a)). It is found from figure 6 that the top plate has strip modes at these frequencies. Radiation ratios predicted from the WFE/BE method will be presented in Section 4 comparing them with the experimental results.

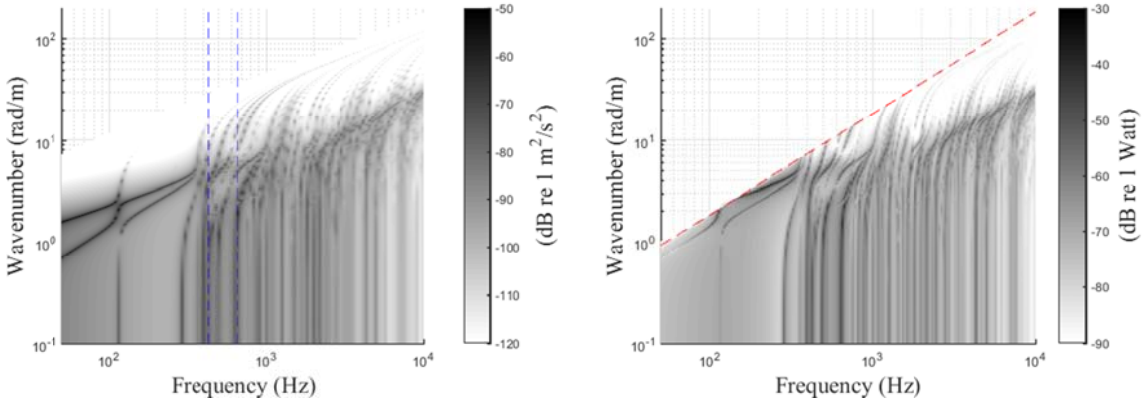

Figure 5. The image plots of (a) the average mean-squared velocity and (b) radiated sound power against frequency and wavenumber for the panel with free boundary conditions. Force excitation at position P3.

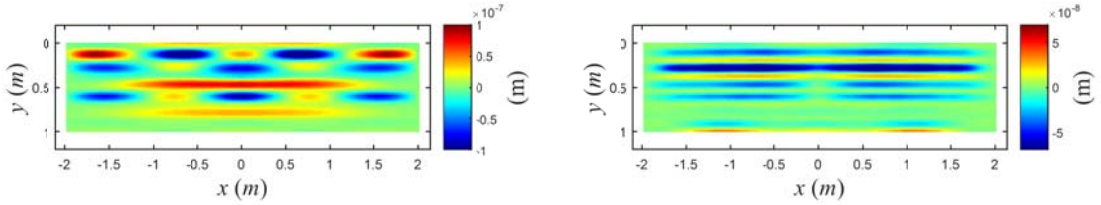

Figure 6. The displacements of the top plates at (a) 428 Hz and (b) 653 Hz in the spatial domain.

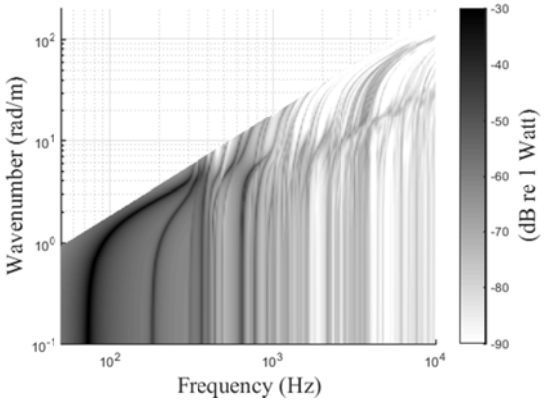

Figure 7. The image plot of transmitted power against frequency and x directional wavenumber for a fixed angle of $\alpha = 90°$ (i.e. $k_y = 0$) and β varying from $0°$ to $90°$.

The transmission coefficient in equation (15) depends on the angle of the incident wave impinging on the top plate as shown in figure 4. The power transmitted through the extruded panel is presented in figure 7 as an image plot for a fixed angle of $\alpha = 90°$ (i.e. $k_y = 0$) and varying β from $0°$ to $90°$ with an interval of $9°$. In the calculation, incident waves were used with a unit pressure amplitude at each incident angle.

Figure 7 shows that incident waves can be transmitted through the panel quite well at low frequencies, especially around 70 Hz where the first global mode wave cuts on. Also, it can be seen that the transmitted power drops considerably at frequencies above 400 Hz where local strip mode waves occur. The transmission loss of the extruded panel predicted by equations (16) and (17) for diffuse sound field will be presented in Section 4 comparing it with that measured from experiments.

4. Validation of numerical results with experiments

In the previous section, the radiation ratio and sound transmission loss of the extruded panel were predicted from the WFE/BE method by assuming that the panel is infinitely long. The results obtained from the WFE/BE approach are compared with those of experiments in this section.

4.1. Experimental set-up

The extruded panel used in the experiment is shown in figure 1(a). This panel has the same cross-section as shown in figure 1(b) and 1(c) and has a length of 1.5m along the extrusion. The experiments for the radiation ratio and sound transmission were done separately with different set-ups. In the case of the radiation ratio, the panel was hung freely with elastic ropes in a reverberation chamber. The

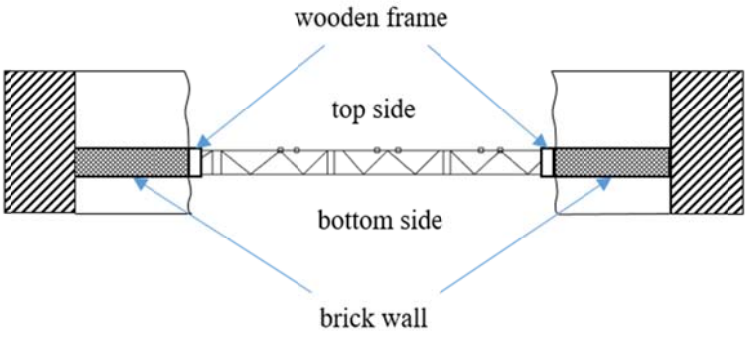

Figure 8. The cross-section of the extruded panel mounted between two reverberation rooms.

radiation ratio of the extruded panel was determined using two different techniques. One is the direct method applying a mechanical excitation to the panel with a shaker. The other one is the reciprocal technique which uses a principle of reciprocity exciting the panel with a loudspeaker within the reverberation chamber and measuring the panel vibration [12].

The experiment for the sound transmission through the extruded panel was conducted between two reverberation chambers in ISVR, University of Southampton UK. The panel was mounted between the two reverberation rooms as illustrated in figure 8. The panel was excited from one room using a loudspeaker and the spatially-averaged sound pressures in each room were measured. The experimental set-ups and post-processing of the results are briefly described in this section; further details are given in reference [5].

4.2. Comparison of numerical and experimental results

In the measurements for radiation ratio, two types of excitation point were chosen on the top plate. One is in the middle of a bay (or a strip), and the other is where a core stiffener is connected. The specific locations of each excitation point are indicated in figure 9. Also, their coordinates are listed in table 2.

First of all, the measured radiation ratios from the direct and reciprocal techniques are compared in figure 10. Figure 10 shows that the two measurement methods give very similar results although there is a bit of level difference at frequencies above 1 kHz in figure 10(a). In addition, figure 10(a) and 10(b) reveal that the excitations at the middle of a strip and a stiffener create fairly different tendencies of the radiation ratio. It seems that the stiffener excitation produces a higher radiation ratio than the strip excitation in general.

The measured two radiation ratios are also compared with the predicted ones in figure 10. As shown in figure 10, the numerical results reveal similar levels and tendencies to the measurements in the high frequency range. According to reference [1], it was shown that the radiation ratio of plates with finite and infinite lengths become close as frequency approaches the coincidence frequency. This

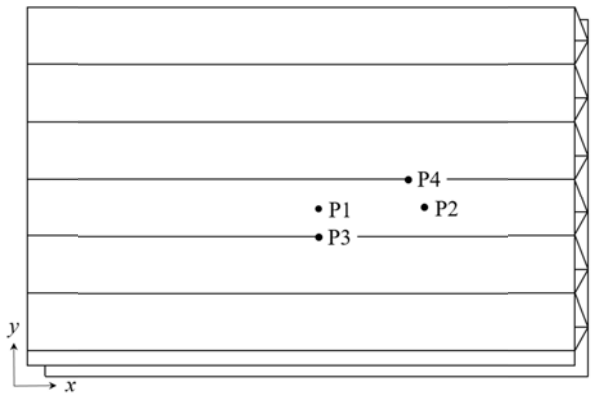

Figure 9. The locations of four excitation points applied on the top plate.

Table 2. The coordinates of excitation points represented in figure 9 (The origin point is at the bottom left hand-corner of the plate).

Excitation point	x (m)	y (m)
P1	0.78	0.472
P2	1.1	0.472
P3	0.78	0.385
P4	1.05	0.54

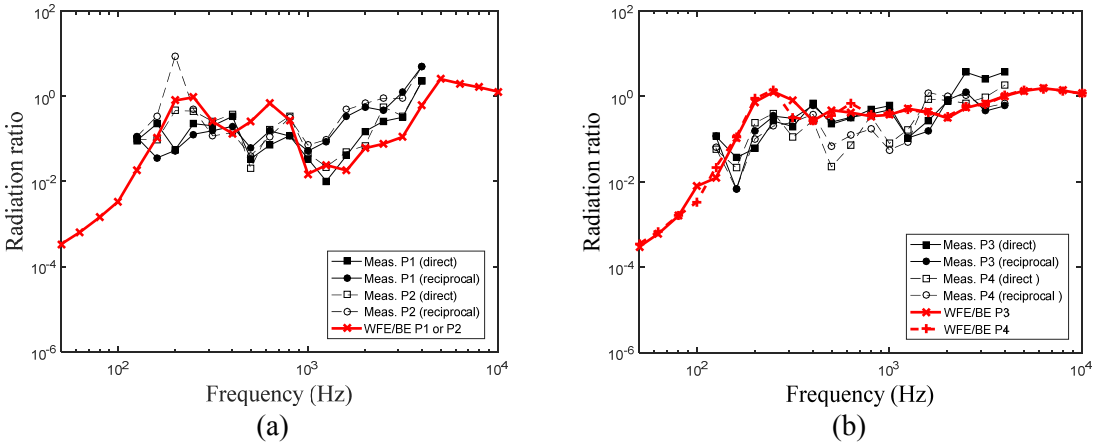

Figure 10. Comparison of radiation ratios obtained from numerical simulation and experiments for (a) strip excitations and (b) stiffener excitations.

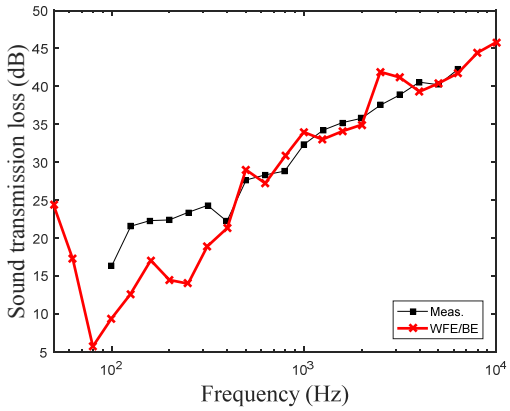

Figure 11. Comparison of sound transmission losses obtained from the numerical simulation and experiment.

behaviour is also observed in figure 10. Additionally, the appearance of localized strip modes in the extruded panel with the finite length seems to contribute to the similarity of levels between the numerical and experimental results at high frequency. Figure 10(a) shows that the experimental results measured by exciting points P1 and P2 are almost the same at frequencies above 400 Hz where the strip modes cut on. From this feature, it can be said that the panel adopted in the present study has a weak influence of size in the *x* direction at frequencies higher than 400 Hz.

The sound transmission loss measured from the experiment is shown in figure 11 together with the predicted one. The numerical result was obtained by diffuse incidences with angles of $0° \le \alpha \le 90°$, $0° \le \beta \le 90°$. It is observed from figure 11 that the measured result shows a discrepancy of about 10dB with the predicted one at low frequencies, below about 400 Hz. However, at frequencies above that, the measured and predicted results agree quite well in level and tendency. As explained already, this agreement at high frequency can be attributed to the occurrence of localized strip modes at high frequencies due to the core stiffeners so that the effects of the finite length of the panel become weaker as frequency increases.

Finally, from the comparison between the measured and predicted results, it is found that the WFE/BE method is quite reliable for predicting the vibro-acoustic behaviour of extruded panels, especially at high frequencies where the conventional FE/BE approach is not applicable. Therefore, it

can be said that the infinite length assumption introduced in the WFE/BE analysis is acceptable even for finite length extruded panels, especially at mid to high frequencies.

5. Conclusions

In this paper, the vibro-acoustic behaviour of a complex shaped extruded panel was investigated by using the wavenumber domain finite and boundary elements (WFE/BE) method. This method assumes that the panel has a uniform cross-section along its length and is infinitely long. The radiation ratio and sound transmission loss were predicted by this numerical method for an extruded panel. Also, in order to validate the numerical method, experiments were conducted with an extruded panel having the same cross-section but a finite length.

For the radiation ratio, two different types of excitation point were selected; in the middle of a strip and where a core stiffener connected in the top plate of the panel. From the comparison with the measured results, it was found that the predicted and measured results show quite similar levels and tendencies. In case of sound transmission, the transmission loss of the panel in diffuse sound field was calculated from the WFE/BE method. It was also found from the comparison with the experiment that the predicted result has a very good agreement with the measured one at frequencies above 400 Hz.

It was observed from the simulation and measurements that the panel used in this study possesses localized deformation trapped in individual strips above 400 Hz. For this reason, the numerical results for the infinite length extruded panel match quite well with the measured ones for the finite length panel at frequencies above 400 Hz.

From this study, it was confirmed that the WFE/BE method is applicable in predicting the vibro-acoustic features of complex extruded panels of finite lengths at mid to high frequencies. It will be helpful to draw design measures improving the vibro-acoustic performances of the extruded panel, particularly for high frequencies where the conventional FE/BE method is not suitable.

Acknowledgments

This research was supported by the Basic Science Research Program through the National Research Foundation of Korea (NRF), funded by the Ministry of Education (2012R1A1A1002779).

References

[1] Xie G, Thompson D J and Jones C J C 2005 The radiation efficiency of baffled plates and strips *Journal of Sound and Vibration* **280** pp 181-209

[2] Prasetiyo I 2012 Investigation of sound transmission in lightweight structures using a waveguide finite element/boundary element approach Ph. D. thesis University of Southampton UK

[3] Orrenius U and Finnveden S 1996 Calculation of wave propagation in rib-stiffened plate structure 2004 *Journal of Sound and Vibration* **198(2)** pp 203-24

[4] Kim H and Ryue J 2014 Sound radiation from strip plates with longitudinal stiffeners using waveguide finite and boundary element methods *Journal of Mechanical Science and Technology* **28(7)** pp 2527-34

[5] Müller A D 2004 Acoustical investigation of an extruded aluminium railway vehicle floor panel M. Sc. thesis University of Southampton UK

[6] Nilsson C M, Thite A N, Jones C J C and Thompson D J 2007 Estimation of sound transmission through extruded panels using a coupled waveguide finite element-boundary element method *Proceedings of the 9th International Workshop on Railway Noise* **99** pp 306-12

[7] Ryue J, Thompson D J, White P R and Thompson D R 2008 Investigations of propagating wave types in railway tracks at high frequencies *Journal of Sound and Vibration* **315** pp 157-75

[8] Ryue J, Thompson D J, White P R and Thompson D R 2009 Decay rates of propagating waves in railway tracks at high frequencies *Journal of Sound and Vibration* **320** pp 955-76

[9] Nilsson C M, Jones C J C, Thompson D J and Ryue J 2009 A waveguide finite element and boundary element approach to calculating the sound radiated by railway and tram rails

Journal of Sound Vibration **321** pp 813-36
[10] Nilsson C M 2004 Waveguide finite elements applied on a car tyre Ph. D. thesis KTH, Stockholm Sweden
[11] Kuttruff H 2000 *Room acoustics* (London: Spon Press) p 55
[12] Squicciarini G, Putra A, Thompson D J, Zhang X and Salim M A 2015 Use of a reciprocity technique to measure the radiation efficiency of a vibrating structure *Applied Acoustics* **89** pp 107-21